

Molecular Dynamics, Fractal Phase-Space Distributions, the Cantor Set, and Puzzles Involving Information Dimensions for Two Compressible Baker Maps.

William Graham Hoover and Carol Griswold Hoover

Ruby Valley Research Institute

Highway Contract 60, Box 601

Ruby Valley, NV 8983

(Dated: January 10, 2020)

Abstract

Nonequilibrium molecular dynamics simulations generate “fractal” [fractional-dimensional] phase-space distributions. Their steady-state “Information Dimensions” are defined by $D_I(\epsilon) = -\sum P(\epsilon) \ln P(\epsilon) / \ln(\epsilon)$. The bin probabilities $\{ P(\epsilon) \}$ are computed using hypercube bins of side-length ϵ . Similarly, with one-dimensional bins, the simplest fractal distribution is the zero-measure 0.630930-dimensional Cantor dust – that singular set of 2^{\aleph_0} points composed solely of ternary 0’s and 2’s. The Cantor dust can be constructed iteratively, by first removing the middle third from the unit interval, next removing the middle thirds of the two remaining segments, then the middle thirds of the remaining four segments, and so on. Because the resulting ordered ternary sets of 0’s and 2’s have the same cardinality as corresponding binary sets of 0’s and 1’s the “02 dust” and the binary “01 continuum” have the “same size” with identical cardinalities, $2^{\aleph_0} \equiv \aleph_1$. With two-dimensional bins we consider two similar linear Baker Mappings, $N2(q, p)$ and $N3(q, p)$. Their “Information Dimensions” D_I , are identical, as estimated from Cantor-like sequential mappings. But the estimates generated by pointwise iteration differ. Further, with $N2$ both these different dimensions disagree with the Kaplan-Yorke dimension D_{KY} based on Lyapunov exponents and thought by most authorities to agree with D_I . The surprising differences among the three $\{ D_I \}$ estimates for $N2$ merit more investigation.

Keywords: Chaos, Lyapunov Exponents, Irreversibility, Random Walks, Maps, Information Dimension

I. NONEQUILIBRIUM MOLECULAR DYNAMICS GENERATES FRACTALS

The computers developed for the National Laboratories were first applied to manybody problems in the 1950s. At Los Alamos in 1953, Fermi, Pasta, and Ulam¹ described the incomplete equilibration of one-dimensional waves in anharmonic chains. Soon afterward, at Livermore, Berni Alder and Tom Wainwright simulated the motion of systems of several hundred hard disks and spheres². At Brookhaven George Vineyard and his coworkers studied “realistic” atomistic models of the impact of high-energy radiation on models of simple metals shortly thereafter³. All of these atomistic simulations were developed based on classical Newtonian mechanics with short-ranged pairwise-additive forces. “Large” simulations involved several hundred discrete particles. A generation later simulations with millions of particles were possible. **Figure 1** shows a typical simulation from our 1989-1990 visit to Japan. The indentation, using two different indenter models, of amorphous Stillinger-Weber silicon, generates plastic flow near the indentors⁴. Trillion-atom simulations are feasible in 2020.

In 1984 Shuichi Nosé announced a revolutionary method for imposing specified temperatures and pressures on molecular dynamics simulations^{5,6}. His modification of Hamiltonian mechanics was designed to replicate Gibbs’ isothermal and isobaric ensembles. Equilibrium distributions had been formulated by Gibbs’ statistical mechanics prior to the close of the 19th century. To match Gibbs’ results Nosé found it necessary to introduce a “scaled” time which had the drawback of introducing wild fluctuations in the dynamics. Hoover helped develop these ideas into practical numerical algorithms⁷ which avoided time-scaling.

Applying the simpler “Nosé-Hoover” ideas to *nonequilibrium* systems (with imposed gradients in temperature or velocity) soon revealed “fractal” (fractional-dimensional) phase-space distributions. These singular distributions provided a mechanistic insight into the genesis of Second-Law *irreversibility* from microscopic *time-reversible* motion equations. While equilibrium Gibbsian distributions are smooth throughout phase space, *nonequilibrium* phase space states were not just less numerous. They had a reduced dimensionality, with states vanishingly rare relative to those familiar from Newtonian and Hamiltonian mechanics.

Although pairwise-additive potentials might seem an oversimplification, work earning Nobel Prizes in chemistry (1986 and 2013), carried out by Dudley Herschbach and Martin Karplus and their colleagues, showed otherwise⁸. Straightforward classical solutions of

pairwise-additive motion turned out to be quite useful in interpreting and predicting the properties of molecules both simple (hydrogen and various alkali halides) and complex (proteins). In most molecular dynamics simulations atomistic trajectories are generated using the “Verlet” or “Störmer” algorithm, with its roots going all the way back to Newton. This algorithm expresses the “next” coordinate value, x_{t+dt} in terms of the previous and current coordinates along with the current value of the acceleration \ddot{x}_t :

$$x_{t+dt} = 2x_t - x_{t-dt} \equiv dt^2(F/m)_t \longleftarrow \ddot{x} = F/m .$$

Runge-Kutta integration of the system of first-order equations,

$$\{ \dot{x} = p_x/m ; \dot{p}_x = F_x \} ,$$

provides better accuracy at a fixed timestep dt , particularly for the velocities. Typical equilibrium simulations, based on Newtonian or Hamiltonian mechanics, use periodic boundary conditions. Series of such simulations can be used to generate “equations of state”, temperature and pressure as functions of energy and density.

Nonequilibrium simulations such as Vineyard’s or the simulation of planar shockwaves require the implementation of special boundary conditions capable of imposing velocity and temperature differences across systems of interest. An early discovery motivating quantitative atomistic simulations was the finding that the width of strong shockwaves is on the order of the size of molecules so that details can be modelled reasonably well with only a few thousand particles. The atomistic and continuum descriptions of strong shockwaves were in rough, ten percent, agreement with one another⁹.

By 1987 a significant difference between equilibrium and nonequilibrium steady states had come to light. Simple nonequilibrium simulations were shown to produce fractal (fractional-dimensional) phase-space distributions, with a negligible phase-space volume relative to corresponding higher-dimensional equilibrium Gibbs’ distributions, such as the microcanonical and canonical ensembles¹⁰⁻¹². About the simplest steady-state mechanical problem results when heat is driven through a Nosé-Hoover harmonic oscillator exposed to a temperature gradient¹³. Where the maximum value of the temperature gradient is ϵ the three motion equations (for the coordinate q , the momentum p , and the current-driving friction coefficient

ζ), are as follows :

$$\dot{q} = p ; \dot{p} = -q - \zeta p ; \dot{\zeta} = p^2 - T(q) ; T(q) = 1 + \epsilon \tanh(q) [\text{NH}] .$$

Here the oscillator mass, force constant, and mean temperature have all been chosen equal to unity. These three coupled equations give rise to a wide variety of solutions. Three such solutions, all for a maximum temperature gradient $\epsilon = 0.42$, are shown in **Figure 2**. We see a dissipative limit cycle as well as two conservative tori. Chaotic solutions are also accessible to the model. More complicated mechanical Models, with two friction coefficients, ζ and ξ , and the same coordinate dependence of the temperature, $T(q) = 1 + \epsilon \tanh(q)$, can generate *ergodic* fractal distributions, solutions which apply for any initial condition. Two examples are shown in **Figure 3**. The Hoover-Holian¹⁴ and Martyna-Klein-Tuckerman¹⁵ motion equations are as follows :

$$\dot{q} = p ; \dot{p} = -q - \zeta p - \xi p^3 ; \dot{\zeta} = p^2 - T(q) ; \dot{\xi} = p^4 - 3p^2 T(q) ; [\text{HH}] ;$$

$$\dot{q} = p ; \dot{p} = -q - \zeta p ; \dot{\zeta} = p^2 - T(q) - \xi \zeta ; \dot{\xi} = \zeta^2 - T(q) ; [\text{MKT}] .$$

The fractal ergodic nature of nonequilibrium states provides a simple explanation for the irreversible behavior (despite time-reversible motion equations) described by the Second Law of Thermodynamics. The fractal strange attractors observed when the equations of motion are solved are not only vanishingly rare states. In addition reversing such a state (by changing the signs of the momentum and the friction coefficients) generates a mechanically-unstable fractal repellor. Because such repellers correspond to *exploding* rather than *collapsing* phase-space objects they are *unobservable*, with negative transport coefficients and entropy destruction rather than production!¹⁰⁻¹².

From a thermodynamic standpoint phase-volume increase corresponds to heating and decrease to cooling. Because irreversible processes necessarily increase heat it follows that a stationary nonequilibrium distribution must extract net heat, leading to the formation of a fractal attractor. A process converting heat to work, a repellor, is outlawed by both the Second Law of Thermodynamics and by computational instability in numerical simulations¹¹.

We consider fractal distributions in more detail in the following Sections. We have already seen that in the 1980s nonequilibrium molecular dynamics led to characterizing of fractal

(fractional dimensional) distributions qualitatively different to Gibbs smooth equilibrium distributions. Because the mathematics of fractals and their geometric characterization is interesting and sometimes paradoxical we highlight interesting research areas well-suited to student exploration in what follows. We begin with the simplest fractal, the Cantor set and a description of its fractal dimensionality. Section III takes up compressible Baker Maps, where phase-volume changes model nonequilibrium heat transfer. The one-way nature of these maps is a direct geometric analog of the Second Law conversion of work to heat. Finally we consider Kaplan and Yorke’s relation linking the fractal information dimension to the Lyapunov exponents. We show that their conjectured equality between the information dimension and the Kaplan-Yorke dimension, $D_{KY} \stackrel{?}{=} D_I$, is precisely true for one Baker map, N3, and definitely false for its very similar twin, N2. This surprise was completely unexpected. It richly deserves further study.

II. THE CANTOR SET AND THE FRACTAL INFORMATION DIMENSION

The simplest fractal is arguably the “middle-third” “Cantor Set” illustrated in **Figure 4**. That set, although equinumerous to the set of real numbers, is full of “holes” and has an information dimension D_I significantly less than that of the reals, 0.630930. The structure of the information dimension of the Cantor set is best seen by considering a base-3 description of the set [those infinite digit strings composed solely of 0’s and 2’s]. Increasing the scale of the description of the set by a factor of 3 (adding one more ternary digit, either 0 or 2) provides only a factor of 2 in the number of new set members in view of the missing digit 1 . D_I is defined and determined from the limiting one-dimensional bin probabilities $\{ P(\epsilon \rightarrow 0) \}$ where the bins have width ϵ :

$$D_I = \sum_{\epsilon \rightarrow 0} P(\epsilon) \ln P(\epsilon) / \ln \epsilon = \ln(2) / \ln(3) = 0.630930 .$$

This simplest of fractals sets the stage for studying two interrelated families of nonequilibrium fractals even simpler than those generated by the conducting harmonic oscillator problems. The two families of simpler Models are [1] stochastic random walks and [2] deterministic time-reversible compressible maps. The expected equivalence of these models is itself interesting. The fact that they can lead to contradictory and paradoxical results,

despite the long history of their study, is currently in need of explanation. The Ian Snook Prize for 2020¹⁶, to be awarded to the author(s) best addressing such an explanation, is designed to shed light on these families of fractal problems.

Sets of points and distributions of density [the latter distribution is often called the “natural measure”] are two representations of “fractals”. Both are well-suited to computational experiments. Our pedagogical example here is the “Cantor set”. An example set member is the base-3 number $0.20220000\dots = 2/3 + 0/9 + 2/27 + 2/81 + 0 = 62/81$. Ambiguity is best reduced by insisting that each set member have an infinitely long digit string with \aleph_0 digits, where \aleph_0 is the number of integers. Because each ternary digit can be either 0 or 2 the Cantor set has $2^{\aleph_0} \equiv \aleph_1$ members. \aleph_0 , the first of Cantor’s transfinite numbers, is the number of integers, and \aleph_1 is the number of real numbers. Evidently \aleph_1 describes, and is the same transfinite cardinality, as that of the set of *all* of the infinitely-long binary-number digit strings between 0 and 1. Each string is constructed entirely of 0’s and 1’s. It is paradoxical, evidently a defect of the mathematics, that the fractal dimensionality of the Cantor set is only $\ln(2)/\ln(3) = 0.630930$ while the equinumerous real numbers have a natural measure of unity and an information dimension of unity.

The information dimension D_I is arguably the most useful descriptor of fractal point sets or distributions. Using the $P \ln P$ formula for $\epsilon = 1/27$ there are eight three-digit members of the Cantor set :

$$\{ 000, 002, 020, 022, 200, 202, 220, 222 \} .$$

The resulting dimensionality is $\ln(1/8)/\ln(1/27) = \ln(2)/\ln(3) = 0.630930$. For any fixed number of digits the same distribution-based result is obtained. A numerical representation of the Cantor set as an arbitrarily-large set of points can be generated by choosing an initial “seed” in the set, like $r = 2/9$ or $r = 62/81$, followed by iteration of the following loop of FORTRAN pseudocode

```
call random_number(ran)
if(ran.lt.1/2) rnew = (r/3)
if(ran.ge.1/2) rnew = (r/3) + (2/3)
r = rnew
```

The FORTRAN `random_number` subroutine generates series of random numbers { `ran` }

uniformly distributed between zero and one. Notice particularly that exactly the same pseudocode describes a random walk with variable length steps. Half the time the walker moves left from his present position r to $r/3$ (corresponding to adding a ternary 0 after the “decimal” point). Otherwise, so also half the time, the walker moves to the right, corresponding to adding in a ternary 2 after the point. The overall single-step operation shifts the ternary representation of r one digit to the right and then chooses randomly either 0 or 2 to precede it.

A distributional representation of the same set can be constructed by removing the middle third from the unit interval, leaving $[0 \text{ to } 1/3]$ and $[2/3 \text{ to } 1]$, then removing the middle thirds of those sets, and so on, repeatedly, with the resulting distribution as is suggested by the multi-million-dot plot of **Figure 4**. Let us up the complexity a bit by turning next to two puzzling two-dimensional mapping problems. Both of them are generalizations of the classic Baker Map.

III. INFORMATION DIMENSIONS FOR COMPRESSIBLE BAKER MAPS

The Baker Map considered by Eberhard Hopf in 1937 provides a simple model for the dissipative chaos responsible for the irreversible behavior of solutions of time-reversible motion equations. By 1987 several examples of thermostated molecular dynamics led to the representation of nonequilibrium steady states as fractal structures in (q, p) (coordinate, momentum) phase space¹⁰⁻¹². A two-panel Baker Map N2, incorporating twofold changes in the area $dqdp$ is the prototypical example, displayed in **Figures 5 and 6**. The mapping¹⁷⁻²⁰ follows the equations

```

if(q-p.le.-sqrt(2/9)) qnew = + (11/ 6)*q - ( 7/ 6)*p + 14*d
if(q-p.le.-sqrt(2/9)) pnew = - ( 7/ 6)*q + (11/ 6)*p - 10*d
if(q-p.gt.-sqrt(2/9)) qnew = + (11/12)*q - ( 7/12)*p - 7*d
if(q-p.gt.-sqrt(2/9)) pnew = - ( 7/12)*q + (11/12)*p - 1*d
[ Nonequilibrium Two-Panel Baker Map N2 ]

```

where the constant d is $\sqrt{1/72}$. The map is irrotational, with unstable fixed points at the top and bottom of the diamond-shaped domain where q is horizontal and p vertical. The diamond-shaped domain has $-\sqrt{2} < q, p < +\sqrt{2}$.

The Nonequilibrium Baker Map N2 is “time-reversible” in the sense that the inverse mapping, $N2^{-1}$ is given by the product mapping $T*N2*T$. The time-reversal mapping T simply changes the sign of the momentum, $T(q, \pm p) = (q, \mp p) = T^{-1}(q, \pm p)$. A typical long-time cumulative solution of the N2 mapping is far from homogeneous but is nonetheless ergodic, with nonvanishing density everywhere within its diamond-shaped domain. This nonequilibrium (area-changing) mapping produces no “holes” so that its box-counting dimension is 2. See the 100 000-point samples of the mapping and its inverse in **Figure 5**. The N2 mapping is compressive parallel to the line $q = p$ and expansive in the perpendicular direction. Numerical work indicates that the resulting distribution of points is random in \tilde{x} and remains fractal in \tilde{y} where the orthogonal coordinates (\tilde{x}, \tilde{y}) occupy a 2×2 square centered on the origin :

$$-1 < \tilde{x} = (q - p)/\sqrt{2} ; \tilde{y} = (q + p)/\sqrt{2} < +1 .$$

For convenience in the measurement of the fractal information and correlation dimensions and the construction of random walks in y corresponding to the fractal direction parallel to $q = p$, it is convenient to map the 2×2 (\tilde{x}, \tilde{y}) square onto the unit (x, y) square :

$$x \equiv (\tilde{x} + 1)/2 ; y \equiv (\tilde{y} + 1)/2 .$$

Then an equivalent set of y values can be generated by a random walk based on random numbers from the unit interval, $0 < \{ r \} < +1$ as follows :

```

call random_number(r)
x = r
call random_number(r)
if(r.lt.(2/3)) ynew = (0+1*y)/3
if(r.ge.(2/3)) ynew = (1+2*y)/3
y = ynew
[ Two-Panel Nonequilibrium Random Walk in the Unit Square, N2 ]

```

Because the N2 mapping and this random walk generate the *same* long-time distributions of the compressive y variable the various fractal dimensions²¹⁻²³ $\{ D \}$ (box-counting, information, Kaplan-Yorke, and correlation, ...) are simply related, $D_{\text{map}}(q, p) = D_{\text{walk}}(y) + 1$.

Careful investigations^{19,20} of the local densities of points in two-dimensional bins of area $\epsilon^2 = (1/3)^{2M}$, with the integer M up to 20, suggested a pointwise fractal information dimension of 1.741_5 . But mapping *regions* rather than *points*, and starting with a uniform distribution in the diamond-shaped domain gave a totally different result ! The information dimension calculated for the same N2 map according to the mapping of regions (areas) rather than by propagation of a single mapped point can be calculated analytically²². The result is $D_{\text{regions}}^{\text{N2}} = 1.789690$ rather than $D_{\text{points}}^{\text{N2}} = 1.741_5$.

A. The Kaplan-Yorke Dimension from Lyapunov Instability

On the other hand – forty years ago – Kaplan and Yorke²⁴ conjectured that the fractal information dimensions of solutions of typical two-dimensional maps are simply related to the solutions' Lyapunov exponents. Because two-thirds of the N2-mapped area undergoes a 1.5-fold stretching while one-third undergoes three-fold stretching the larger Lyapunov exponent is $\lambda_1 = (2/3) \ln(3/2) + (1/3) \ln(3) = +0.636514$. The smaller (negative) Lyapunov exponent describes the shrinking: $\lambda_2 = (2/3) \ln(1/3) + (1/3) \ln(2/3) = -0.867563$. Kaplan and Yorke reasoned that the information dimension for such a map is given by

$$D_I = 1 - (\lambda_1/\lambda_2) = 1.7337 ,$$

a bit less than the estimate from bin-density data^{19,20} and far from the analytic area-mapping result, 1.789690 .

In our efforts to understand these differences we came upon a related N3 mapping, compared to N2 in **Figure 6**. N3 is a slight elaboration of N2, and from the standpoint of irrotational area mappings produces the same information dimension. Here is the FORTRAN description of a single step in the corresponding Random Walk :

```

call random_number(r)
x = r
call random_number(r)
if (r.lt.(2/3))                ynew = (y/3) + (0/3)
if((r.ge.(2/3)).and.(r.le.(5/6))) ynew = (y/3) + (1/3)
if (r.gt.(5/6))                ynew = (y/3) + (2/3)
y = ynew
[ Three-Panel Nonequilibrium Random Walk, N3 ]

```

Throughout our numerical work we have used the handy FORTRAN random-number generator indicated here, “`random_number(r)`”, said to have a repeat length of order 10^{77} .

To illustrate the differences in ordering of the bin populations resulting from the fourth steps of the random walks equivalent to N2 and N3 we compare million-point 81-bin histograms of the two Walks in **Figures 7 and 8**. Evidently the N3 mapping, starting with a uniform distribution, produces exactly the same set of bin probabilities as does N2 (though in a different order) and so the walks have exactly the same information dimensions²², 0.789690. But in the N3 case the Lyapunov exponents, and the Kaplan-Yorke dimension, are different, and produce an interesting surprise :

$$\lambda_1 = (2/3) \ln(3/2) + (1/3) \ln(6) = 0.867563 ; \lambda_2 = (2/3) \ln(1/3) + (1/3) \ln(1/3) = -1.098612 .$$

$$\rightarrow D_{KY} = 1 - (\lambda_1/\lambda_2) = 1.789690 . [\text{Equivalent to } D_I \text{ for N3}] .$$

In fact *this time* the Kaplan-Yorke conjecture is true, provided one imagines that the steady state maintains the stationary value of the information dimension observed during the evolution suggested by **Figure 9** ! A proof or disproof of this thought would be welcome.

IV. DISCUSSION AND CONCLUSIONS

The Kaplan-Yorke conjecture $D_I \stackrel{?}{=} D_{KY}$ is forty years old. It is surprising that the simple counterexample for the linear N2 mapping considered here evaded detection for so many years. We have seen that the generalized Baker Maps N2 and N3 agree with both the thermodynamic and the computational statements of the Second Law of Thermodynamics. The Baker Map fractals provide exactly the same computational mechanism for dissipation as is present in manybody simulations. But our understanding remains incomplete. Why *is* or *is not* the Kaplan-Yorke approximation valid or invalid for linear maps? The puzzling difference between pointwise dimensionality and regionwise dimensionality is likewise unsettling, but is firmly established by our results.

The mathematics of fractal sets remains paradoxical and challenging. Besides the disagreement between the various versions of the information dimension the simple geometry of fractals is itself puzzling. The popular understanding of cumulus clouds as 2.5-dimensional objects suggests that fractals are isotropic. The Sierpinski carpet and sponge fractals have characteristic rotational symmetries. On the other hand *all* of the fractals arising from statistical mechanics appear to be anisotropic. Particular local directions correspond to exponential instability or stability. Without anisotropy there could be no Kaplan-Yorke analysis of dimension. The unsettling cardinality equivalence of the holey Cantor dust and the holeless continuum, despite their different information dimensions, suggests that there is much more work for the mathematicians to do, perhaps with useful physical applications.

In any event a thorough pedagogical explanation of the situation described here will help to understand these issues. Such an explanation has been set as the 2020 Ian Snook Prize Problem recently described in Reference 16.

-
- ¹ J. Ford, “The Fermi-Pasta-Ulam Problem: Paradox Turns Discovery”, *Physics Reports* **213**, 271-310 (1992).
- ² B. J. Alder and T. E. Wainwright, “Molecules in Motion”, *Scientific American* **201**(4), 113-130 (1959).
- ³ J. B. Gibson, A. N. Goland, M. Milgram, and G. H. Vineyard, “Dynamics of Radiation Damage”, *Physical Review* **120**, 1229-1253 (1960).
- ⁴ W. G. Hoover, A. J. DeGroot, C. G. Hoover, I. Stowers, T. Kawai, B. L. Holian, T. Boku, S. Ihara, and J. Belak, “Large-Scale [millions of atoms] Elastic-Plastic Indentation Simulations *via* Nonequilibrium Molecular Dynamics “*Physical Review A* **42**, 5844-5853 (1990).
- ⁵ S. Nosé, “A Unified Formulation of the Constant Temperature Molecular Dynamics Methods”, *Journal of Chemical Physics* **81**, 511-519 (1984).
- ⁶ S. Nosé, “A Molecular Dynamics Method for Simulations in the Canonical Ensemble”, *Molecular Physics* **100**, 191-198 (2002).
- ⁷ W. G. Hoover, “Canonical Dynamics: Equilibrium Phase-Space Distributions”, *Physical Review A* **31**, 1695-1697 (1985).
- ⁸ M. Karplus, “ ‘Spinach on the Ceiling’ : a Theoretical Chemist’s Return to Biology”, *Annual Review of Biophysics and Biomolecular Structure* **35**, 1-47 (2006).
- ⁹ B. L. Holian, W. G. Hoover, B. Moran, and G. K. Straub, “Shockwave Structure *via* Nonequilibrium Molecular Dynamics and Navier-Stokes Continuum Mechanics”, *Physical Review A* **22**, 2798-2808 (1980).
- ¹⁰ B. Moran, W. G. Hoover, and S. Bestiale, “Diffusion in a Periodic Lorentz Gas”, *Journal of Statistical Physics* **48**, 709-726 (1987).
- ¹¹ B. L. Holian, W. G. Hoover, and H. A. Posch, “Resolution of Loschmidt’s Paradox: The Origin of Irreversible Behavior in Reversible Atomistic Dynamics”, *Physical Review Letters* **59**, 10-13 (1987).
- ¹² W. G. Hoover, H. A. Posch, B. L. Holian, M. J. Gillan, M. Mareschal, and C. Massobrio, “Dissipative Irreversibility from Nosé’s Reversible Mechanics”, *Molecular Simulation* **1**, 79-86 (1987).
- ¹³ J. C. Sprott, W. G. Hoover, and C. G. Hoover, “Heat Conduction, and the Lack Thereof, in

- Time-Reversible Dynamical Systems. Generalized Nosé-Hoover Oscillators with a Temperature Gradient”, *Physical Review E* **89**, 042914 (2014).
- ¹⁴ W. G. Hoover and B. L. Holian, “Kinetic Moments Method for the Canonical Ensemble Distribution”, *Physics Letters A* **211**, 253-257 (1996).
- ¹⁵ C. J. Martyna, M. L. Klein, and M. Tuckerman, “Nosé-Hoover Chain—the Canonical Ensemble *via* Continuous Dynamics”, *Journal of Chemical Physics* **97**, 2635-2643 (1992).
- ¹⁶ W. G. Hoover and C. G. Hoover, “2020 Ian Snook Prize Problem: Three Routes to the Information Dimensions for One-Dimensional Stochastic Random Walks and Their Equivalent Two-Dimensional Baker Maps”, *Computational Methods in Science and Technology* **25**, 153-159 (2019).
- ¹⁷ W. G. Hoover and H. A. Posch, “Chaos and Irreversibility in Simple Model Systems”, *Chaos* **8**, 366-373 (1998)
- ¹⁸ J. Kumičák, “Irreversibility in a Simple Reversible Model”, *Physical Review E* **71**, 016115 (2005).
- ¹⁹ W. G. Hoover and C. G. Hoover, “Aspects of Dynamical Simulations, Emphasizing Nosé and Nosé-Hoover Dynamics and the Compressible Baker Map”, *Computational Methods in Science and Technology* **25**, 125-141 (2019).
- ²⁰ W. G. Hoover and C. G. Hoover, “Random Walk Equivalence to the Compressible Baker Map and the Kaplan-Yorke Approximation to Its Information Dimension”, arXiv:1909.04526 (2019).
- ²¹ C. Grebogi, E. Ott, and J. A. Yorke, “Roundoff-Induced Periodicity and the Correlation Dimension of Chaotic Attractors”, *Physical Review A* **38**, 3688-3692 (1988).
- ²² J. D. Farmer, “Information Dimension and the Probabilistic Structure of Chaos”, *Zeitschrift für Naturforschung* **37 A**, 1304-1325 (1982).
- ²³ J. D. Farmer, E. Ott, and J. A. Yorke, “The Dimension of Chaotic Attractors”, *Physica* **7D**, 153-180 (1983).
- ²⁴ J. L. Kaplan and J. A. Yorke, “Chaotic Behavior of Multidimensional Difference Equations”, pages 204-227 in *Functional Differential Equations and the Approximation of Fixed Points*, edited by H. O. Peitgen and H. O. Walther (Springer, Berlin, 1979).

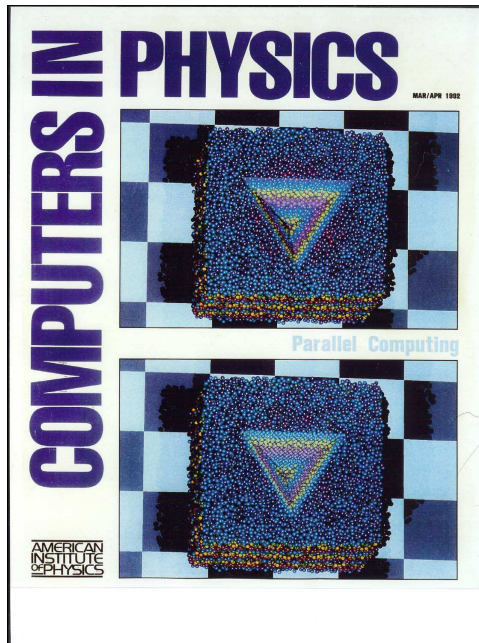


FIG. 1: This 1992 cover illustrates two 32 768-atom indentations of amorphous silicon, one with a smooth-faced tetrahedral indenter, the other with a rough face-centered-cubic atomistic indenter. See Reference 4 for the details. By 2020 simulations with trillions of atoms became feasible.

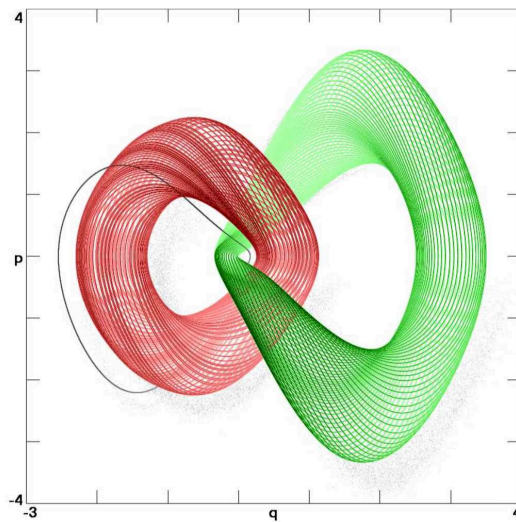


FIG. 2: Three stationary solutions for the Nosé-Hoover oscillator with maximum temperature gradient $\epsilon = 0.42$. See Reference 13 for more details.

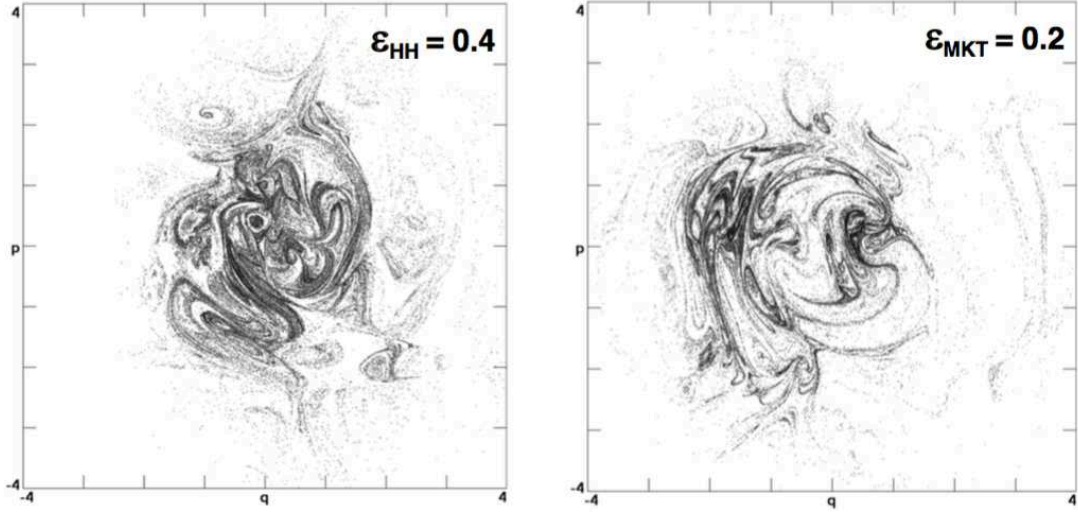


FIG. 3: Two fractal $p(q)$ sections near the $\zeta = \xi = 0$ plane for [left] the Hoover-Holian Oscillator with $\epsilon = 0.40$ and for [right] the Martyna-Klein-Tuckerman Oscillator with $\epsilon = 0.20$. See Section 5.7.2 of W. G. Hoover and C. G. Hoover’s *Simulation and Control of Chaotic Nonequilibrium Systems* (World Scientific, Singapore, 2015).

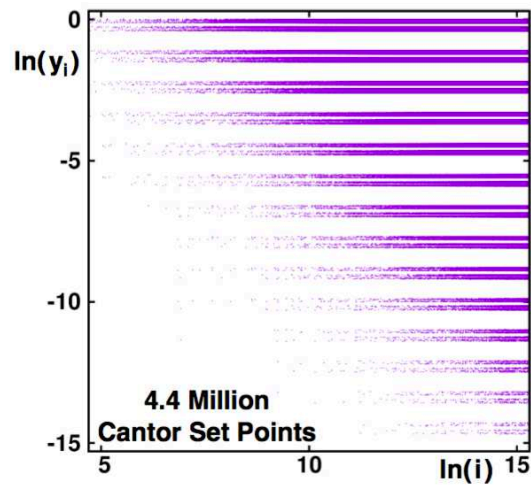


FIG. 4: 4.4 million representative points y_i from the Cantor dust. The set of largest horizontal gaps corresponds to the smallest “middle thirds” $\{ (1/3)^n \text{ to } (2/3)^n \}$ which are excluded from the dust.

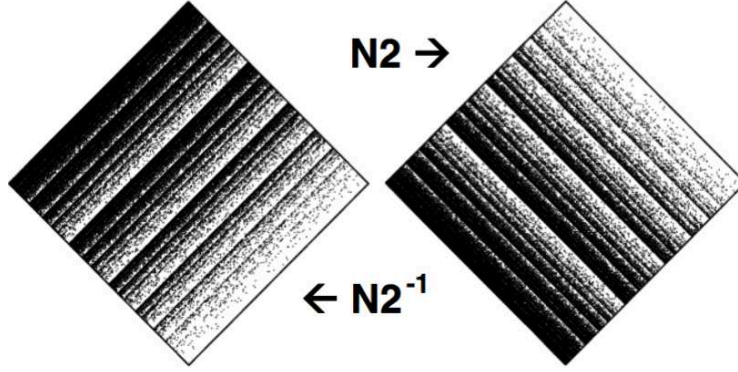


FIG. 5: The repeller generated by $N2^{-1}$ (at left) and attractor generated by $N2$ (at right) using 100 000 iterations from the initial point $(q, p) = (0, 0)$. Note that $-\sqrt{2} < q, p < +\sqrt{2}$.

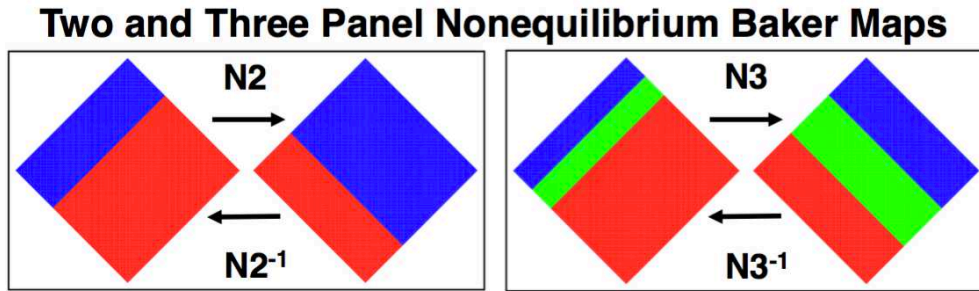


FIG. 6: The rotationless two-panel and three-panel maps $N2$ and $N3$ are illustrated here. For more details see our recent arXiv contributions.

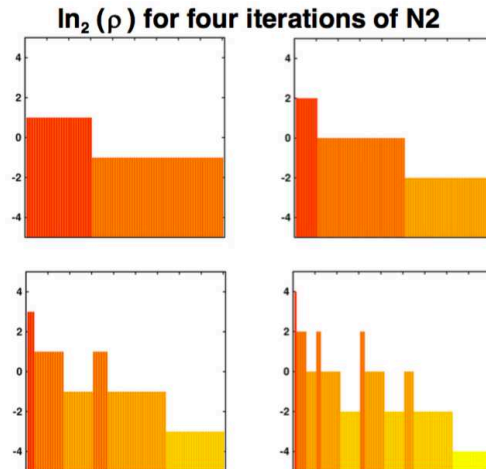


FIG. 7: The histograms resulting from four iterations of the random walk version of the $N2$ map. The initial distribution of one million points was uniform in the interval $(0, 1)$. The logarithms of the bin probabilities show five steps of height $\ln(4)$. At the fourth iteration the numbers of bins at each step, from the highest probability to the lowest, are $\{ 1 \times 1, 2 \times 4, 4 \times 6, 8 \times 4, 16 \times 1 \}$.

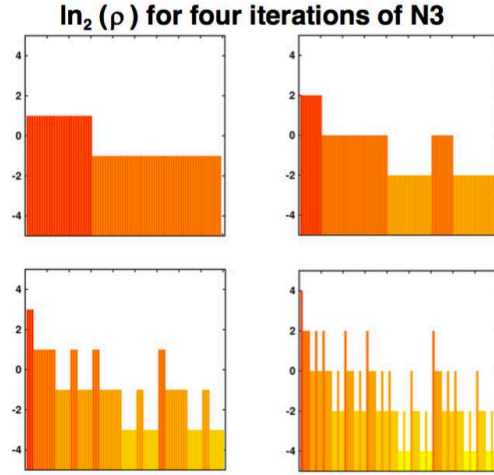


FIG. 8: The histograms resulting from four iterations of the random walk version of the N3 map. The initial distribution of one million points was uniform in the interval (0,1). The logarithms of the bin probabilities show five steps of height $\ln(4)$. At the fourth iteration the numbers of bins at each step, from the highest probability to the lowest, are exactly the same as those from the N2 mapping in **Figure 7**.

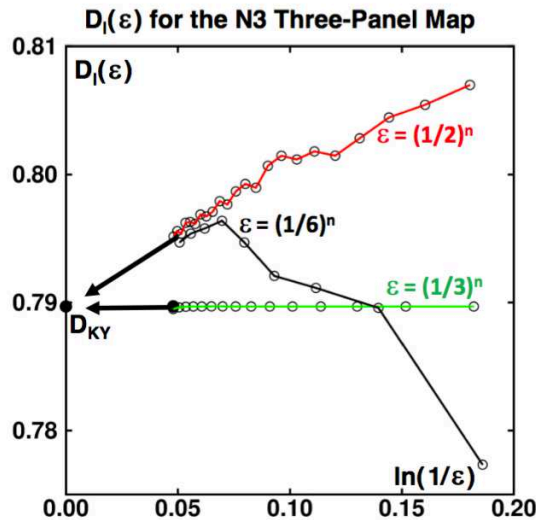


FIG. 9: Information Dimension data for the random walk problem equivalent to the N3 Mapping are all consistent with the same information dimension $D_I = D_{KY} = 0.789690$ for the Walk and 1.789690 for the Mapping. Pointwise analyses of the N3 mapping are described here for meshes of $(1/2)^n$ (red), $(1/3)^n$ (green), and $(1/6)^n$ (black). Analogous data for the N2 mapping are displayed in Figure 5 of Reference 16.